Polyhedron 176 (2020) 114277

Contents lists available at ScienceDirect

Polyhedron

journal homepage: www.elsevier.com/locate/poly

The role of methyl and benzyl substituted dithiocarbazate of 2-acetyl pyridine for the formation of bridged dimeric and unbridged monomeric copper(II) complexes and catecholase mimetic activity of the complexes

Ananyakumari Santra [a], Paula Brandao [b], Gopinath Mondal [a], Pradip Bera [a,c], Abhimanyu Jana [a], Indranil Bhattacharyya [a], Chandana Pramanik [a,d], Pulakesh Bera [a,*]

[a] Department of Chemistry, Panskura Banamali College (Autonomous), Panskura R.S, Midnapore (East), West Bengal 721152, India
[b] CICECO, University of Aveiro, 3810-193 Aveiro, Portugal
[c] Kandi College, Murshidabad, West Bengal 742137, India
[d] Department of Chemistry, Dinabandhu Andrews College, Garia, Kolkata, West Bengal 700084, India

ARTICLE INFO

Article history:
Received 7 September 2019
Accepted 1 December 2019
Available online 16 December 2019

Keywords:
Cu(II) complex
X-ray crystallography
London dispersion
DFT
Catecholase activity

ABSTRACT

Monomeric $[Cu(L_1)Cl]$ (**1**) and dimeric $[Cu(L_2)Cl]_2$ (**2**) copper(II) complexes, where HL_1 = methyl-2-(1-(pyridine-2-yl)ethylidene)-hydrazine-1-carbodithioate and HL_2 = benzyl-2-(1-(pyridine-2-yl)ethylidene)hydrazine-1-carbodithioate, have been synthesized and characterized by X-ray crystallography, TGA and spectral methods. Complex **1** crystallizes in a space group *P*21/n and adopts a square planar environment surrounding the Cu ion, and complex **2** is a triclinic crystal system with space group Pī. Complex **2** is a centrosymmetric dimer where each copper atom forms two chloro bridges and completes five coordination with the tridentate NNS donor. Density functional calculations demonstrate that chloro-unbridged structure of **1** is favored by London dispersion between its layers. It is noticed that the layers are usually packed closely in the solid phase, such attractive interactions are sterically hindered between the layers of **2.** Due to the presence of large phenyl group that extend from one layer to the other, the layers cannot slide on top of each other. This leads to the chloro-bridged structure of **2** stabilized by electrostatic interactions between Cu and Cl atoms located at different layers. Both complexes exhibit prominent catecholase activity in methanol following the oxidation of 3,5-di-*tert*-butyl catechol (DTBC) to the corresponding quinone. Based on the observed turn over frequency of **1** (25.19 h^{-1}) and **2** (10.76 h^{-1}), the monomeric complex demonstrates more catechol mimetic oxidation than the dimer. A plausible mechanism of catecholase activity has been discussed.

1. Introduction

Schiff bases derived from S-alkyl/aryl dithiocarbazates are a very important class of NSS chelating agents which allow the formation of stable complexes with a wide range of transition and non-transition metal ions [1–5]. These metal complexes have been shown to exhibit interesting electronic behaviors like non-linear optics [6,7], magnetic [8], electrochemical properties [9] and chemotherapeutic properties [10]. Among the reported complexes, the monomeric complexes are numerous whereas the polynuclear complexes are particularly rare. Recently, dinuclear copper(II) complexes of Schiff bases 2-benzoylpyridine S-methyldithiocarbazate and di-2-pyridyl ketone N(4),N(4)-(butane-1,4-diyl) thiosemicarbazone have been synthesized and structurally characterized [5,11,12]. M. R. P. Kurup reported the synthesis and structural characterization of a dinuclear copper(II) complex of di-2-pyridyl ketone N(4),N(4)-(butane-1,4-diyl) thiosemicarbazone [13]. Very recently Koo reported the structure and chemistry of a dinuclear copper(II) complex derived from mixed ligand of benzoic acid and 2-acetylpyridine/2-benzoylpyridine based benzhydrazide [14]. Both monomer and dinuclear copper(II) entities of 2-pyridinecarbaldehyde thiosemicarbazone have been reported to show antiferromagnetism and nuclease activity [8]. G. Fenteany et al. reported the synthesis and structure activity relationship in the cancer cell proliferation study of both monomer and dimeric complexes of M(II) (M = Cu and Zn)-Schiff's bases derived from 2-acetyl pyridine and S-alkyl dithiocarbazates [2]. The reports on several biological applications such as antimicrobial activity [4], cytotoxicity effect [15,16], biocatalytic [17–19], and antiproliferative [20] have been shown by these class of compounds. Design and synthesis of efficient bio-inspired, environ-

* Corresponding author.
E-mail address: pbera.pbc.chem@gmail.com (P. Bera).

https://doi.org/10.1016/j.poly.2019.114277
0277-5387/

ment friendly catalysts that mimic enzymatic activities are also very crucial in synthetic and supramolecular chemistry. The enzymes active sites are modeled with the metal complexes using the knowledge of redox behavior and coordination chemistry. S-alkyl/aryl derived metal complexes are not frequently modeled though these are bioactive compounds [1–5]. The geometry and the structural features of enzyme active sites and the choice of metal binding can be helpful to establish the structure–function activities in the model experiments [21,22]. Several copper based mononuclear and dinuclear complexes have been modeled to study insight about the mechanism of the biological oxidation process of 3,5-di-*tert*-butylcatechol (DTBC) to 3,5-di-*tert*-butylquinone (DTBQ) [23–26]. Herein, we report the synthesis, characterization and theoretical interpretation in relative stability of a mononuclear copper(II) complex of deprotonated methyl-2-(1-(pyridin-2-yl)ethylidene)hydrazine-1-carbodithioate (HL_1) and a dinuclear dichloro bridged copper(II) complex of deprotonated benzyl-2-(1-(pyridin-2-yl)ethylidene)hydrazine-1-carbodithioate (HL_2), and investigate their ability to catalyze catechol oxidase mimetic activity. The stability of the complexes and their tendency toward chloro-bridged and chloro-unbridged structures were investigated by B3LYP-D3 calculations [27–29].

2. Experimental section

2.1. Materials

Reagent grade metal salts $CuCl_2{\cdot}2H_2O$ was purchased from Merck India and used without further purification. Hydrazine hydrate (99%), carbon disulfide, benzyl chloride, methyl iodide, and 2-acetyl pyridine were purchased from Merck chemical company and used without further purification. Solvent ethanol (Changshu Yangyuan Chemical, China), methanol (Merck, India) and dichloromethane (Merck, India) were dried and distilled before use in the experiment.

2.2. Synthesis of methyl-2-(1-(pyridine-2-yl)ethylidene)hydrazine-1-carbodithioate (HL_1) and benzyl-2-(1-(pyridine-2-yl)ethylidene) hydrazine-1-carbodithioate (HL_2)

The HL_1 and HL_2 were prepared by the condensation of 2-acetyl pyridine with corresponding hydrazine carbodithioate [2,30]. Methyl hydrazine carbodithioate and benzyl hydrazine carbodithioate were synthesized from 99% pure hydrazine hydrate, carbon disulfide, and methyl iodide. The freshly prepared methyl hydrazine carbodithioate (10 mmol, 1.22 g) was refluxed with 2-acetyl pyridine (10 mmol, 1.21 g) in dry methanol for half an hour to obtain methyl-2-(1-(pyridin-2-yl)ethylidene)hydrazine-1-carbodithioate (HL_1). The crude product of HL_1 was crystallized from 1:1 ethanol–water. Yield: 2.01 g (89%). Elemental analyses (%) for $C_9H_{11}N_3S_2$ are C, 47.97; H, 4.92; N, 18.65; S, 28.46%. Found C, 47.69; H, 4.89; N, 18.56; S, 28.48%. Similarly, benzyl-2-(1-(pyridin-2-yl)ethylidene)hydrazine-1-carbodithioate (HL_2) was prepared following the condensation of benzyl hydrazine carbodithioate (10 mmol, 1.98 g) and 2-acetyl pyridine (10 mmol, 1.21 g) in methanol. The crude product thus obtained was crystallized from 1:1 ethanol–water. Yield: 2.57 g (73.79%). Elemental analyses (%) for $C_{15}H_{15}N_3S_2$ are C, 59.77; H, 5.02; N, 13.94; S, 21.27%. Found C, 59.62; H, 4.91; N, 13.85; S, 21.30%.

2.3. Synthesis of copper complexes

Copper(II) complexes **1** and **2** were synthesized by the reaction of the methanolic solution of HL_1 and HL_2 with copper chloride, respectively [2]. Separately HL_1 (10 mmol, 2.25 g) and HL_2 (10 mmol, 3.01 g) were allowed to react with $CuCl_2{\cdot}2H_2O$ (10 mmol, 1.70 g) in methanol. The reaction mixture in each case was stirred for 3 h at room temperature and then refluxed for 2 h in a water bath. In both the cases, solid deep green product was separated out which is filtered and washed with dry methanol. The solid products were dried over silica-gel. A pinch of solid products was taken in 1:1 methanol-DMF and placed the solution in the open air for slow evaporation. Deep blue micro crystals suitable for single crystal X-ray analysis were grown. Yield for **1** is 2.50 g (77.4%). Elemental analyses (%) for $C_9H_{10}N_3S_2ClCu$ (**1**) are C, 33.43; H, 3.12; N, 13.0; S, 19.83%. Found C, 33.39; H, 3.10; N, 13.01; S, 19.88%. Yield for **2** is 6.2 g (77.52%). Elemental analyses (%) for $C_{30}H_{28}N_6S_4Cl_2CuN_6S_4$ (**2**) are C, 45.11; H, 3.53; N, 10.52; S, 16.05%. Found C, 45.01; H, 3.47; N, 10.45; S, 16.08%.

2.4. Characterization

FISONS EA-1108 CHN analyzer was used for elemental analysis (C, H, N, and S) of the ligands and complexes. The FTIR spectra (4000–500 cm^{-1}) were recorded on a Perkin Elmer Spectrum Two FT-IR Spectrophotometer with sample prepared as KBr pellets. Mass spectra of ligands were obtained using a Waters HRMS XEVO-G2QTOF#YCA351. Thermogravimetric analysis was performed using Perkin Elmer Thermal Analyzer TGA4000 instrument at a heating rate 20 °C/min under nitrogen atmosphere. The X-band electron paramagnetic resonance (EPR) spectrum was recorded in a Bruker EMX X-band spectrometer operating at a field modulation of 100 kHz, modulation amplitude of 7 G and microwave radiation power of 10 mW at room temperature. The single crystal X-ray diffractions of complex **1** and **2** were carried out on a Bruker SMART APEX II X-ray diffractometer equipped with graphite-monochromated Mo-Kα radiation (λ = 0.71073 Å) and 16 CCD area detector. The intensity data were collected in the π and ω scan mode, operating at 50 kV, 30 mA at 296 K [31]. The data reduction was performed using the SAINT and SADABS programs [32]. All calculations in the structural solution and refinement were performed using the Bruker SHELXTL program [33]. The structure was solved by the heavy atom method and refined by full-matrix least-squares methods. All the non-hydrogen atoms were refined anisotropically; the hydrogen atoms were geometrically positioned and fixed with isotropic thermal parameters. The final electron density maps showed no significant difference.

The catecholase activities of **1** and **2** were examined by the reaction of 100 equivalents of 3,5-di-*tert*-butylcatechol (DTBC) with 1×10^{-5} M solutions of the complexes under aerobic conditions at ambient temperature in methanol. The reaction was followed spectrophotometrically by monitoring the growth of the absorbance as a function of time at *ca.* 400 nm which is characteristic of 3,5-di-*tert*-butylquinone chromophore. To determine the dependence of the rate of the reaction on substrate concentration and to evaluate various kinetic parameters, 1×10^{-5} M solutions of the complexes were mixed with at least 10 equivalents of the substrate to maintain pseudo-first order condition. To check the rate dependency on catalyst concentrations similar set of experiments were performed at a fixed concentration of substrate with various catalyst concentrations. The rate of a reaction was determined by the initial rate method, and the average initial rate over three independent measurements was recorded.

2.5. Computational details

All calculations were performed with the ORCA 4.0 program package [34,35] by using def2-TZVP and its matching auxiliary basis sets [36,37]. The structures were fully optimized at the unrestricted Kohn-Sham B3LYP [27–29] level of density functional theory (DFT) calculations incorporating the atom-pairwise dispersion

correction (D3) with Becke–Johnson damping (BJ) [38], i.e., UB3LYP-D3(BJ), within the resolution of identity (RI) approach RIJ-COSX [39,40]. The effect of methylene solution on the energetics was assessed implicitly at the same level of theory through the conductor-like polarizable continuum model (C-PCM) [41].

The molecular docking was carried out using AUTODOCK 4.0 software as accomplished by the graphical user interface AUTODOCK TOOLS 4.0 (AD4.1_bound.dat). The macro cyclic receptor was choosing as PDB formed of three dimensional x-ray crystals structure of a Truncated ErbB2 Ectodomain Reveals an Active Conformation (entry 2A91 in the Protein Data Bank). The graphical user interface AUTODOCK TOOLS was devoted to setup the protein: water molecule was deleted from the crystal of protein, only polar hydrogen were added, computed gasteigers charge was calculated as −10.998 and non polar hydrogen were merged to carbon atom. Complexes 3D structures were saved in PDB format with the aid of the program MERCURY. The AUTODOCK TOOLS program was used to make docking input file. A grid box size for complex **1** is 83 × 85 × 83 and complex **2** is 74 × 74 × 82 with grid spacing 1 Å. Both receptor and complex were save pdbqt format. A distances-dependent functions of the dielectric constant were used for the calculation of the energetic map. Ten runs were generated by using Lamarckian genetic algorithm searches. Default settings were used with an initial population of 50 randomly placed individuals, a maximum number of $2.5x10^6$ energy evaluations [42]. Final docking was run with autogrid4.exe and autodock4.exe function to generate glg and dlg files respectively. The graphical interactions picture were found using Schrodinger software.

3. Result and discussion

3.1. Chemistry

Ligands have a proton adjacent to the thiocarbonyl group and consequently can exhibit thione-thiol tautomerism (Scheme 1). Mostly the structure of the reported complexes derived from Schiff bases of S-alkyl/aryl dithiocarbazate adopted monomeric structure [1–5]. The formation of the monomer from methyl ester (HL_1) and dimer from benzyl ester (HL_2) of dithiocarbazic acid suggest that SR group has a pronounced effect on nuclearity and structure of the complexes. Mass spectra of **1** and **2** show *m*/*z* value 286.96 and 363.02, respectively, which correspond to a highly unsaturated $[ML]^+$ species (Fig. S1 for **1** and Fig. S2 for **2**). The $[CuL_1]^+$ from **1** is further attached with another NNS donor (L_1) to satisfy its maximum coordination number (6) forming $[Cu(L_1)_2]^+$ giving *m*/*z* value 509. In the mass spectrum of **2**, no peak equivalent to the dichloro-bridged complex is obtained but a peak *m*/*z* value 763.21 is observed which can be assigned as the chloro-bridged complex, $[Cu_2(L_2)_2Cl]^+$. Solid state FTIR spectra analysis was performed to determine the coordination mode of the ligand with the copper (II) ion (Fig. S3). The FTIR spectra do not display any ν_{S-H} band at *ca.* 2600 cm^{-1}, but exhibit ν_{NH} bands in the range 3100–3200 cm^{-1} indicating that the ligands remain in the thio-keto tautomer in the solid state. The significant differences in spectral data were analyzed by comparing the spectra of the complexes with the corresponding ligand shown in Table S1. The $\nu_{NH/NH2}$ stretching vibrations of the ligand HL_1 and HL_2 appeared at 3138 and 3154 cm^{-1}, respectively. These higher frequency peaks are not observed in the complex indicating the involvement of primary or secondary amine during the complexation. The observed ν_{C-N}, $\nu_{C=N}$ and $\nu_{C=S}$ stretching frequencies of the corresponding ligand and complexes appear at the range of 1408–1496 cm^{-1}, 1585–1708 cm^{-1} and 770–784 cm^{-1}, respectively. The characteristic stretching frequencies of $\nu_{C=N}$ and $\nu_{C=S}$ shifted to higher frequencies upon complexation indicating the coordination of nitrogen and sulfur atoms to the copper(II) ion [43].

3.2. TGA analysis

As can be seen in Fig. 1, the decomposition profile of the ligand HL_1 and HL_2 are very similar. Both are stable up to 150 °C and major decomposition occurs between 150 °C and 330 °C. The first step of decomposition is attributed to the loss of the SR unit. Almost all the organics evaporates completely at 300 °C. The decomposition profile proves that ligands are quite suitable for the formation of stable complexes. Complexes (**1** and **2**) also decomposed following very similar decomposition pattern. Both **1** and **2** are stable up to 250 °C. A weight loss about 14.5% and 15.4% correspond to the loss of one unit of SCH_3 and one unit SCH_2-Ph in **1** and **2**, respectively. Complex **1** starts decomposition at 220 °C. In the first step of decomposition 15 unit mass loss corresponds to a loss of CH_3 from SCH_3 of the ligand. The major loss of organics and coordinate Cl atom occur between 250 °C and 350 °C. If heating is continued more than 800 °C the gradual weight loss will happen until CuS (29.53%) is obtained i.e., leading to the formation of CuS. The analysis indicated that complex **1** is a suitable single-source precursor for CuS particle synthesis.

3.3. EPR spectroscopy

The EPR spectroscopy is a powerful tool to study the electronic and magnetic properties of the metal center. Generally Cu(II) complexes are distorted octahedral geometry (tetragonal or rhombic). An axially symmetric more intense peak at higher field ($g_{\|}$) and

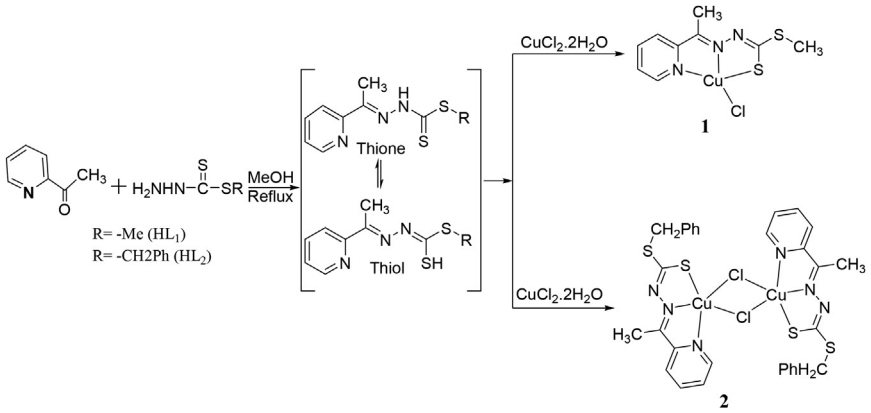

Scheme 1. Formation pathway of HL_1, HL_2, 1 and 2.

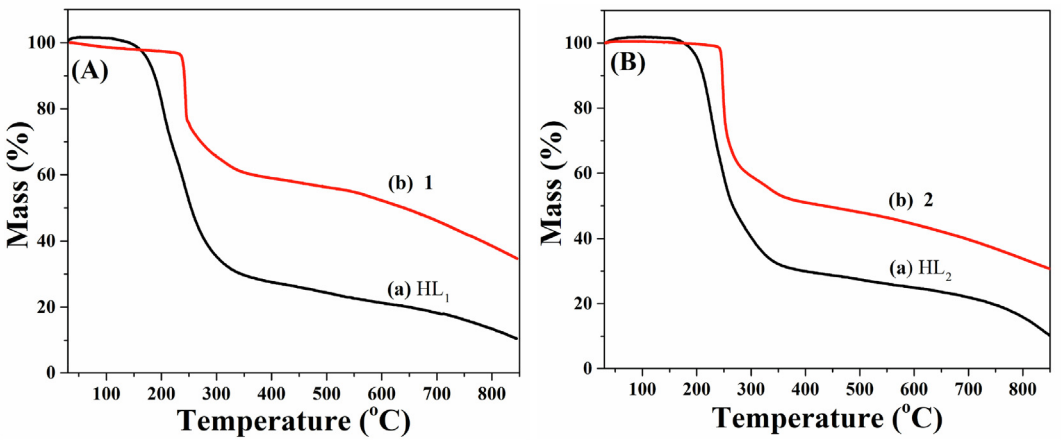

Fig. 1. Thermogravimetry analysis of HL_1 and **1** (A); HL_2 and **2** (B).

low intense peak at lower field ($g^{\perp}$) are observed for Cu(II) complexes [44]. The X-band EPR spectrum of the solid SP1 sample at RT shows classical resonance bands of axial symmetry with $g_{\parallel}$ = 2.097 (A = 91 G) and $g^{\perp}$ = 2.047 as shown in Fig 2.

A rhombic distorted EPR spectrum is observed for the solid SP2 sample at RT with $g_{\parallel}$ = 2.12 and $g^{\perp}$ = 2.06 without any signature of nuclear coupling between two copper(II) ions. So, it can be concluded that the unpair electron is highly localized in d_{x2-y2} orbital of Cu(II) ion. The similar results are also found in the literature [45,46].

3.4. Single crystal X-ray analysis

To establish the structure and coordination environment of the synthesized complexes single crystal X-ray analysis of the complexes were performed. The crystal refinement data of the reported complexes are given in Table 1. An ORTEP view of **1** with atom leveling scheme of the independent past is shown in Fig. 3 and a selection of bond angles and length is given in Table 2 and Table 3. The metal ion in **1** possesses approximate square planer geometry with pyridinyl nitrogen donor, an imine nitrogen donor and sulfur atom of cabodithioate unit, and a chloride ion. Complex **1** is a monomeric complex and crystallizes in the monoclinic P 21/n space group in approximate square planer geometry. Bond angles N1–Cu–N2, N2–Cu–S1, N1–Cu–Cl1 and Cl1–Cu–S1 are 80.06(4)°, 84.69(3)°, 97.32(3)° and 97.81(2)°, respectively (Table 2) whereas N1–Cu–S1 and Cl1–Cu–N2 angles are 176.53(3)° and 164.50(3)°, respectively. The measured dihedral angle 3.24° corresponds to Cu-S1-C8-N3-N2 and Cu-N2-C6-C5-N1 planes to a planer geometry

Table 1
Crystal refinement parameters of the complexes **1** and 2.

	1	**2**
CCDC	1833374	1833376
Moiety formula	$C_9H_{10}ClCuN_3S_2$	$C_{30}H_{28}Cl_2Cu_2N_6S_4$
Mr	323.31	798.82
a(Å)	8.1368(11)	7.9812(11)
b(Å)	8.7126(10)	8.4000(11)
c(Å)	17.106(2)	13.8741(18)
α(°)	90	93.512(4)
β(°)	101.547(4)	106.006(4)
γ(°)	90	113.715(4)
Crystal system	monoclinic	Triclinic
Volume (Å^3)	1188.2(3)	802.77(19)
Space group	*P*21/n	P ī
Z	4	1
F (0 0 0)	652.0	406.0
Dcalc (g cm^{-3})	1.807	1.652
Absorption coefficient / μ(mm^{-1})	2.387	1.784
h,k,l	11,12,24	10,11,19
2θ	61.15	58.58
Reflections I > 2σ(I)	3349	3595
Total reflections I > 2σ(I)	3645	4332
R1(I > 2σ(I))	0.0206	0.0444
w*R2*(all reflections)	0.0551	0.1192
goodness_of_fit	1.057	1.079
Residuals (e.Å3)	0.471/-0.585	1.288/-0.972

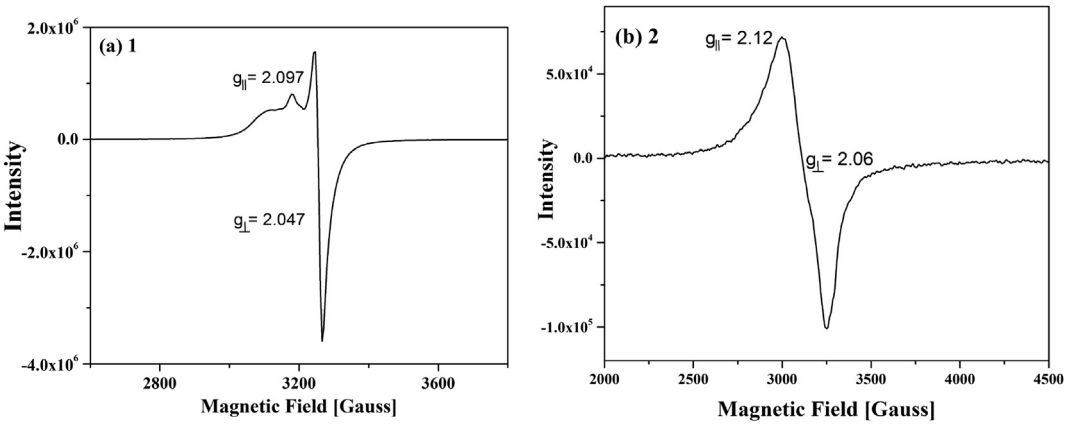

Fig. 2. Soilid state EPR spectrum of 1 (a) and 2 (b).

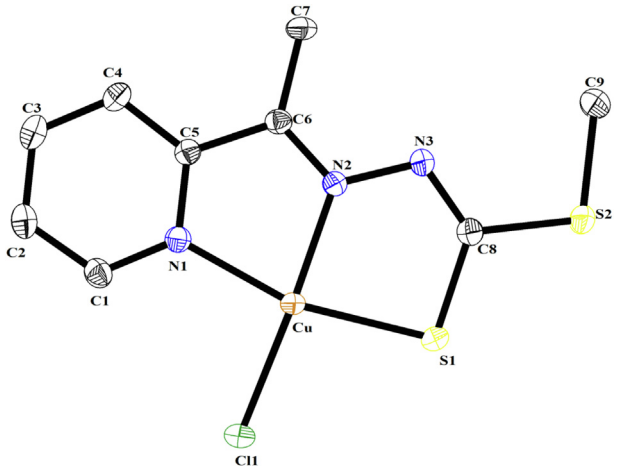

Fig. 3. ORTEP picture of the complex **1**. Thermal ellipsoids are drawn at the 55% probability label. For the clarity of the structure hydrogen atoms have been omitted. Structure truncated to highlight the ligand–metal bonding geometry.

Table 2
Selected bond lengths of **1** and **2**.

Atoms	**1** Length (Å)	**2** Length(Å)
Cu–Cl1	2.2166(5)	2.2595(8)
Cu–S1	2.2615(4)	2.2659(7)
Cu–N1	2.031(1)	2.032(2)
Cu–N2	1.960(1)	1.966(2)
Cu–Cl1′	–	2.711(1)
S1–C8	1.737(1)	1.734(3)
S2–C8	1.744(1)	1.747(3)
S2–C9	1.801(1)	1.830(3)
N1–C1	1.337(2)	1.337(4)
N1–C5	1.357(2)	1.359(3)
N2–N3	1.384(1)	1.391(3)
N2–C6	1.296(1)	1.299(3)
N3–C8	1.305(1)	1.311(3)

Symmetry code for Cl1′ = 1 − x, 2−y, 1−z.

Table 3
Selected bond angles of **1** and **2**.

Atoms	**1** Angle (°)	**2** Angle (°)
Cl1–Cu–S1	97.81(2)	96.63(3)
Cl1–Cu–N1	97.32(3)	97.08(7)
Cl1–Cu–N2	176.53(3)	171.69(8)
S1–Cu–N1	164.50(3)	162.35(7)
S1–Cu–N2	84.69(3)	84.73(7)
N1–Cu–N2	80.06(4)	80.1(1)
Cu–S1–C8	94.16(4)	94.0(1)
Cu–N1–C1	127.89(9)	128.0(2)
Cu–N1–C5	112.86(8)	112.6(2)
Cu–N2–N3	122.93(8)	122.8(2)
C8–S2–C9	102.59(6)	–
S1–Cu–Cl1	–	101.26(3)
N1–Cu–Cl1	–	89.62(7)
N2–Cu–Cl1	–	96.97(7)
Cu–N2–C6	118.60(8)	
Cu–Cl1–Cu	–	89.19(3)
N3–N2–C6	118.4(1)	–
Cl1–Cu–Cl1	–	90.81(3)

which confirms nearly square planar geometry of the complex with τ4 value 0.9. There is no H-bonding interaction but strong aromatic-π and chelate-π (3.432 Å/3.567 Å) interaction form a supramolecular arrangement (Fig. 4). The calculated offset angle between two centroids planes is 2.12°. The selective bond lengths Cu–N1, Cu–N2, Cu–Cl1 and Cu–S1 are 2.031(1)°, 1.960(1)°, 2.2166 (5)° and 2.2615(4)°, respectively, as shown in Table 3. The similar length and angle of bis-chelated complexes of a dithiocarbazate N, S Schiff base ligand were observed [47]. The relatively shorter bond lengths of copper-nitrogen i.e., Cu–N1 (2.031 Å) and Cu–N2 (1.960 Å) than the reported copper(I) complexes are strongly suggesting the presence of copper in +2 state in the reported complexes [48]. The corresponding Cu^{+2}–N bond lengths (2.073 and 2.019 Å) of **1** calculated presently at the UB3LYP-D3 level are also quite consistent with the X-ray values. The corresponding BVS (Bond Valence Sum) calculation is also supportive to planar structure with 2.26 (Table S2).

In the presence of copper(II) chloride salt ligand HL_2 furnished a chloro-bridged binuclear Cu(II) complex. Fig. 5 shows the single crystal X-ray structure of the complex **2**. It has a triclinic crystal system with Pī space group. In complex 2, the two symmetry related copper atoms exhibit a penta coordinated bridged environment. The uninegative L2 ligand coordinate the copper atom through the pyridinyl N, imine N and thiolato sulfur donors and the two copper atoms are connected by a pair of chloride bridge. Of the doubly bridging Cl atoms, one occupies the basal plane and the other is located at the apical position of the square pyramidal geometry, indicated by the index τ5 value 0.2 [49,50]. The Cu–N1 and Cu–N2 bond lengths of **2** are 2.032(2) Å and 1.966(2) Å, respectively. These are analogous to the respective bond lengths of **1**, and thus are consistent with the + 2 oxidation state of copper atoms. The higher value of Cu–Cl1 bond (2.2595Å) in **2** is due to the Jhan-Teller distortion in d^9 system. The UB3LYP-D3 calculations on the dimeric **2** find the corresponding Cu^{+2}–N bond lengths as 2.064 and 2.006 Å, which are consistent with the X-ray values revealing oxidation state + II. The BVS value (2.17) of **2** is also supportive the + 2 oxidation state of copper (Table S2). In the complex, strong aromatic-π ↔ chelate-π (3.558 Å) and chelate-π ↔ chelate-π (3.618 Å) interaction make a stable supramolecular array shown in Fig. 6. The calculated offset angle between two centroids planes is 6.08°.

3.5. Computational results

1 and **2** have monomeric and dimeric chloro-bridged structures in their single crystals, respectively. Computationally, both the monomeric and dimeric structures for both complexes in the gas phase and in the solution can be obtained to access the experimen-

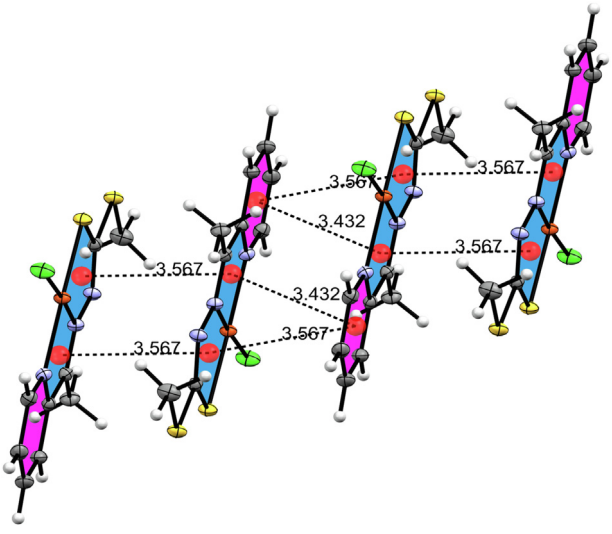

Fig. 4. Aromatic-π and chelate-π interactions in complex **1**.

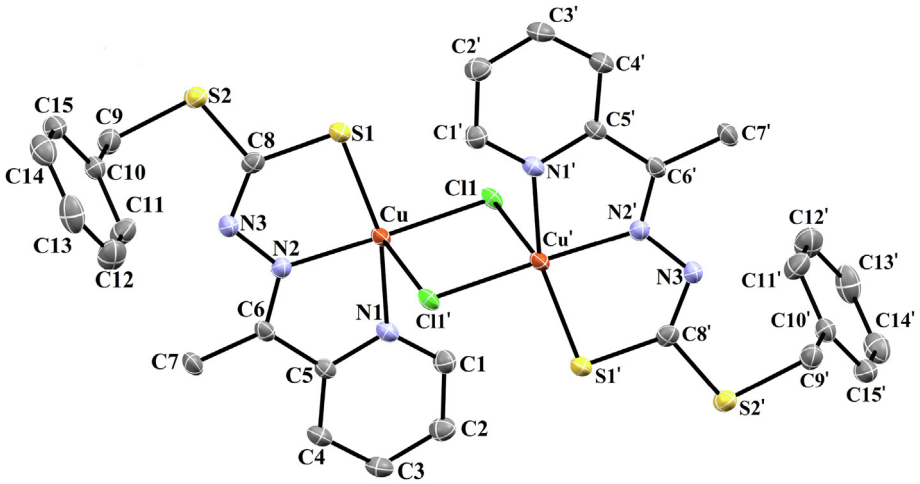

Fig. 5. ORTEP diagram of **2**. Thermal ellipsoids are drawn at the 55% probability label. For the clarity of the structure hydrogen atoms have been omitted. Structure truncated to highlight the ligand–metal bonding geometry.

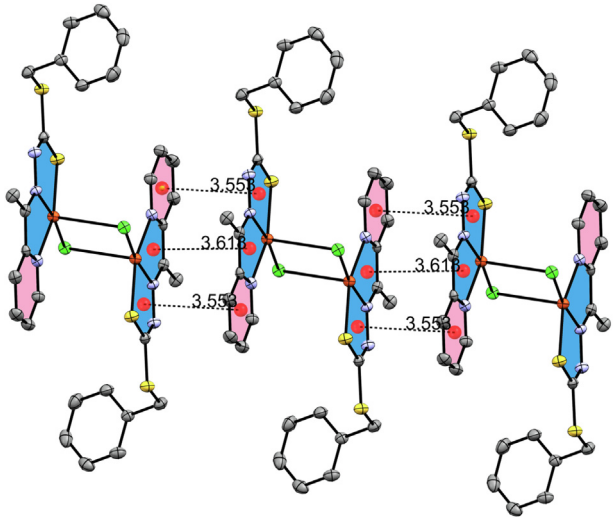

Fig. 6. Aromatic-π and chelate-π interactions in **2**.

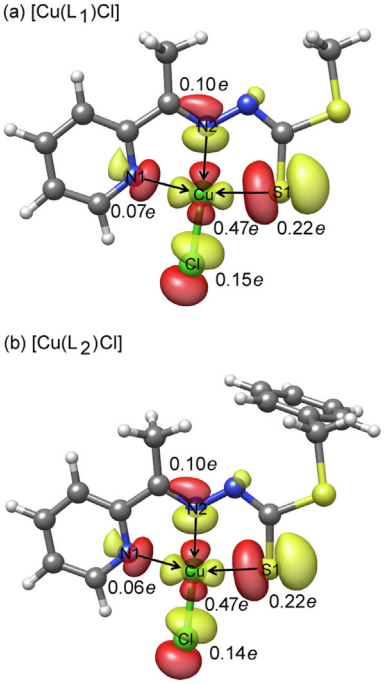

Fig. 7. Singly-occupied orbital of monomeric **1** and **2** and the associated atomic Mulliken spin densities calculated at the UB3LYP.

tal preference of one structure over the other. In this study, the stability of the monomeric and dimeric complexes of **1** and **2** has been investigated by the UB3LYP-D3 calculations. As shown in Fig. 7, the monomeric structures of **1** and **2** have one-unpaired electron (doublet state), which is primarily located on the $CuCl^{+}$ moiety (with largest spin density on the Cu^{+2} ion), consistent with the results on analogous Cu(II) complexes [51]. The coordinating atoms S1, N1, and N2 have also noticeable spin densities.

The single unpaired electron of monomeric **1** and **2** can couple in the dimeric structures in parallel and anti-parallel configurations, yielding triplet and open-shell singlet spin states, respectively. The triplet states of the dimers of both **1** and **2** (1 kcal/mol) are more stable than the singlet states at the UB3LYP level. The smallness of the singlet–triplet energy gap is consistent with the previous studies on analogous Cu(II) complexes [52]. The spin density distributions of all dimeric structures are identical to those of the monomeric structures. However, as expected, in the open-shell singlet state of the dimeric structures, atomic spin densities have opposite signs on both fragments. Therefore, we do not provide them additionally in Fig. 7. As seen in Table 4, the gas-phase UB3LYP calculations find almost the same binding energies with both ligands (~−255 kcal/mol). The stabilizing dispersive interaction components of the binding energy are noticeable (~−10 kcal/mol) but much smaller than the overall binding energy. Although methanol weakens the interaction greatly (~115 kcal/mol), the coordination of the ligands to $CuCl^{+}$ is still strong in solution (~−152 kcal/mol). As the ligands coordinate to the $CuCl^{+}$ ion with nearly the same energies, their preference to monomeric and dimeric structure formation cannot be assigned to the differences in their electronic structure.

To shed light on the dimerization process of [Cu(L_1)Cl] and [Cu(L_2)Cl] complexes, first we optimized the geometry of the chloro-bridged [Cu(L_2)Cl]$_2$ complex at the UB3LYP-D3 level by taking the initial coordinates from the present X-ray structure. It should be noted here that other stable dimeric structures can be obtained when the initial orientations of the two layers are different. However, our aim is not to explore conformational space of the dimers

Table 4
The calculated binding energies (ΔE, kcal/mol) for the interaction of the $CuCl^+$ ion with the anionic L_1 and L_2 ligands and for the interaction of the two identical $[Cu(L_1)Cl]$ and $[Cu(L_2)Cl]$ complexes together with their individual components for UB3LYP level bare gas-phase interaction (ΔE_{UB3LYP}), its D3-level dispersion correction ($\Delta E_{D3\text{-}disp}$), and UB3LYP level solvent effect ($\Delta E_{UB3LYP\text{-}solv}$).

	ΔE	ΔE_{UB3LYP}	$\Delta E_{D3\text{-}disp}$	$\Delta E_{UB3LYP\text{-}solv}$
Doublet monomer				
$[L1^-\cdots CuCl^+]$	−151.7	−258.3	−10.0	116.5
$[L2^-\cdots CuCl^+]$	−151.4	−255.4	−10.9	114.9
Triplet dimer				
$[Cu(L_1)Cl]\cdots[Cu(L_1)Cl]$	−21.0	0.2	−33.1	11.9
$[Cu(L_2)Cl]\cdots[Cu(L_2)Cl]$	−16.6	−10.8	−19.0	13.2
Singlet dimer				
$[Cu(L_1)Cl]\cdots[Cu(L_1)Cl]$	−18.4	1.4	−31.0	11.2
$[Cu(L_2)Cl]\cdots[Cu(L_2)Cl]$	−16.7	−11.7	−17.3	12.2

but to assess the factors that differentiate the preference of the ligands towards chloro-bridged and chloro-unbridged structures when the layers are initially oriented parallel as in the X-ray structure of $[Cu(L_2)Cl]_2$. The optimized coordinates of $[Cu(L_2)Cl]_2$ are consistent with the X-ray coordinates. As can be seen in Fig. 8(a), the chloro-bridged crystal structure of $[Cu(L_2)Cl]_2$ is preserved.

By replacing the two SCH_2Ph moieties of the X-ray structure of $[Cu(L_2)Cl]_2$ with the SCH_3 moieties, we obtained initial coordinates for the chloro-bridged $[Cu(L_1)Cl]_2$ complex. However, the two layers in the initial coordinates of the $[Cu(L_1)Cl]_2$ complex slide over each other during geometry optimization due to strong attraction between Cl atom and methyl group of 2-acetyl pyridine belonging to different $[Cu(L_1)Cl]$ layers, as seen in Fig. 8(b). Therefore, the chloro-bridged structure is not preserved for the $[Cu(L_1)Cl]$ dimer. The resulting computational structure of this dimer is consistent with the X-ray structure shown in Fig. 5. Since SCH_3 moiety of L_1 is small, the $[Cu(L_1)Cl]$ layers can slide on top of each other easily.

The same type of strong interaction is also expected for $[Cu(L_2)Cl]$ dimer. However, the size of the phenyl moiety is larger than the distance between the $[Cu(L_2)Cl]$ layers. Therefore, the $[Cu(L_2)Cl]$ layers cannot slide on top of each other despite the strong attraction between Cl atom and methyl group of 2-acetyl pyridine, which leads chloro-bridged $[Cu(L_2)Cl]_2$ structure. Methanol solution

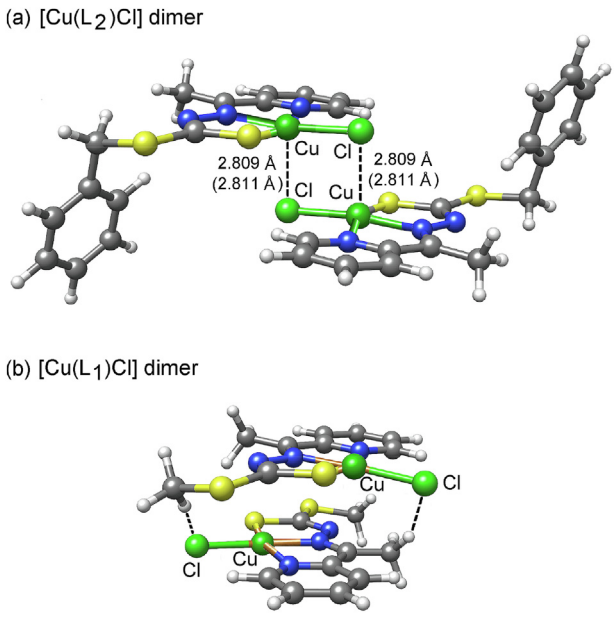

Fig.8. B3LYP-D3 optimized structure of $[Cu(L_2)Cl]_2$ starting from its X-ray coordinates, and of $[Cu(L_1)Cl]_2$ starting from the X-ray coordinates of $[Cu(L_2)Cl]_2$ after replacing both SCH_2Ph moieties with SCH_3 moieties.

weakens the interaction energy of the two layers of the dimeric structures by ~12 kcal/mol. In the absence of solution, the gas-phase UB3LYP-D3 interaction energy of the layers with both ligands are ~−30 kcal/mol (the sum of UB3LYP and D3 contributions in Table 4). The interaction between the two layers of $[Cu(L_1)Cl]_2$ is slightly repulsive without dispersion contribution. Therefore, the chloro-unbridged $[Cu(L_1)Cl]_2$ structure is driven mainly by the favored London dispersion in addition to the stabilizing electrostatic interaction between the Cl and CH_3 moieties of the two layers. Methyl group is already well known as a dispersion energy donor [53].

The interaction between the two layers of the chloro-bridged $[Cu(L_2)Cl]_2$ is already strong (~−12 kcal/mol) without dispersion contribution at the UB3LYP-D3 level, owing to the strong electrostatic interaction between the two CuCl moieties. The dispersion contribution in the chloro-bridged $[Cu(L_2)Cl]_2$ is also significant but ~10 kcal/mol smaller than that in the chloro-unbridged $[Cu(L_1)Cl]_2$.

These indicate that the stabilities of both chloro-bridged and chloro-unbridged structures are governed largely by the electrostatics and London dispersion. When the layers cannot slide on top of each other due to the large size of the SCH_2Ph tail of the L_2 ligand, electrostatic interaction between the two layers becomes the main stabilizing effect through the formation of the chloro-bridged structure, followed by London dispersion. However, with L_1 ligand having small SCH_3 tail, the Cl and CH_3 moieties of the two layers are attracted to each other due to strong dispersion interaction, which breaks the chloro-bridge.

3.6. Catechol oxidase mimetic activity

Catechol oxidases are ubiquitous plant enzymes containing a dinuclear copper center. To study the catalytic mechanism model complexes **1** and **2** catalyze the oxidation of 3,5-di-^{t}butyl catechol (DTBC) to 3,5-di-*tert*-butyl-*o*-quinone (DTBQ) coupled with the reduction of oxygen to hydrogen peroxide. DTBC has lower redox potential that facilitates the oxidation of DTBC and the bulky substituent prevents further reactions such as ring-opening process. Here we introduced analogous copper complexes of NNS donor ligands (**1** and **2**) to check the catecholase activity in the air. The presence of the labile group (Cl) makes metal centre susceptible to ligand's substitution. Various approaches have been reported by a different group to investigate the mechanism pathway of DTBC oxidation by model copper complexes [54,55]. The product DTBQ is quite stable in air and has a characteristic transition at about 400 nm and therefore the catalytic study can be monitored by UV–Vis spectrophotometry. Reactivity and kinetic studies were performed in methanol because of the good solubility of the complexes, substrate and their product in this solvent. Before going to the detailed kinetic investigation, it is first necessary to check the

ability of the complexes to behave as catalysts for the catechol oxidase mimetic activity. Accordingly, 1.0×10^{-5} M solutions of the complexes were treated with a 200-fold concentrated solution of DTBC, and the spectra were recorded up to 1.5 h in dioxygen saturated methanol at room temperature. The time dependent spectral changes for a period of 1.5 h after the addition of DTBC are displayed in Fig. 9 for **1** and **2**. The spectral scan reveals the increase of the band intensity at *ca.* 400 nm characteristic of quinine chromophore for both complexes although a blank experiment using copper chloride salt instead of the complexes did not show significant spectral growth. These results suggest that **1** and **2** are active towards the catecholase activity.

The initial rate of reactions versus concentration of the substrate data show a first-order rate dependence on the substrate concentration at lower concentrations of DTBC but almost zero order at the higher concentrations (Fig. 10). This observation suggests that quinone formation proceeds through a relatively stable intermediate, a complex-substrate adduct, followed by the irreversible redox transformation of the intermediate at the rate determining step. In this regard, the Michaelis-Menten model is helpful to explain the rate saturation kinetics on the concentration of the substrate. The observed initial rates versus substrate concentration plot and the Lineweaver–Burk plot for both complexes are shown in Fig. 11. Analysis of the experimental data produced Michaelis binding constant (K_M) values of 1.733×10^{-4} M for **1** and 1.01×10^{-3} for **2** and V_{max} values of 6.999×10^{-8} M s^{-1} and 2.991×10^{-8} M s^{-1} for **1** and **2**, respectively (Table 5). The turnover frequency (K_{cat}) value is obtained by dividing the V_{max} by the concentration of the catalyst used and is found to be 25.19 and 10.76 h^{-1} for **1** and **2**, respectively. Previous studies on catecholase activities of copper complexes showed wide range of k_{cat} values 1 to 9471 h^{-1} [44]. The observed k_{cat} values of 25.19 h^{-1} for **1** and 10.76 h^{-1} for **2** are comparable to those with moderate catecholase activities [54–56].

The mass spectra of complexes with DTBC are performed to establish the possible mechanism catalytic oxidation. The plausible catalytic cycle is given in Scheme 2. Mass spectra of monomer (**1**) and dimer (**2**) in $CDCl_3$ show the existence of $[ML]^+$ species which can be attributed to the formation of the highly solvated intermediate product following a dissociative mechanism. The peaks corresponding to $[CuL]^+$ are observed at *m*/*z* 287.5 (Fig. S1) and *m*/*z* 363.91 (Fig. S2) for **1** and **2**, respectively. An intense peak with *m*/*z* value 509 in **1** is also observed which can be assigned as $[Cu(L_1)_2]^+$. The formation of stable $[Cu(L_1)_2]^+$ is the result of the reorganization of $[CuL]^+$ with another ligand unit through solvent displacement mechanism. The intermediate $[CuL]^+$ activates

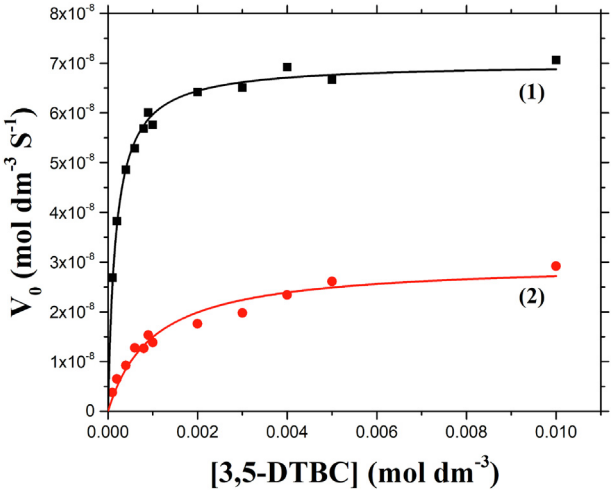

Fig. 10. Initial rate versus substrate concentration plot for the oxidation of 3.5-DTBC in air-saturated methanol catalyzed by the complexes at room temperature. Symbols and solid lines represent the experimental and simulated profiles, respectively.

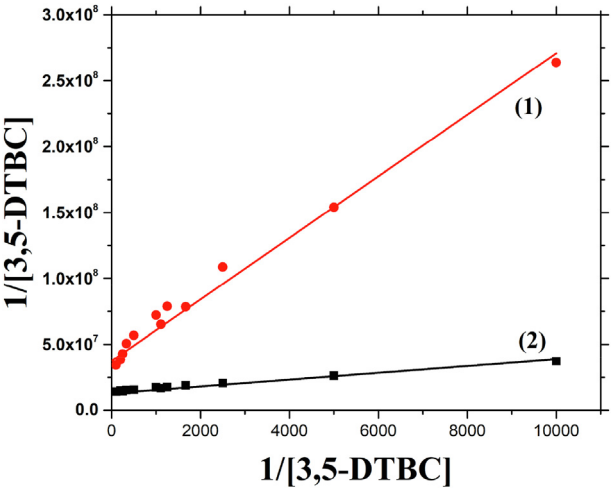

Fig. 11. Line weaver–Burk plots for the oxidation of 3,5-DTBC catalyzed by **1** and **2** in methanol. Symbols and solid lines represent the experimental and simulated profiles, respectively.

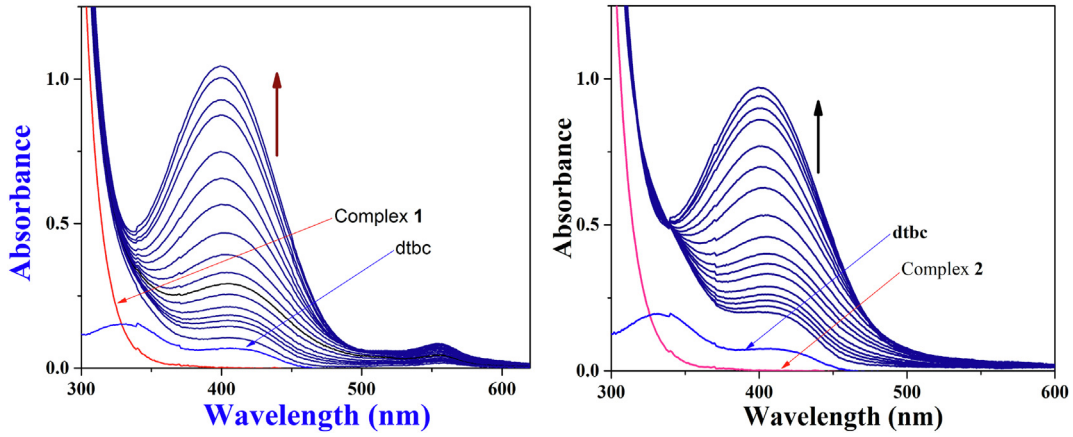

Fig. 9. The spectral profile showing growth of 3,5-DTBQ at 400 nm upon addition of 0.001 M 3,5-DTBQ to a solution containing **1** (1×10^{-5} M) in methanol. The spectra were recorded in 5 min time interval in aerobic condition at room temperature.

Table 5
Kinetics data and k_{cat} values of **1** and **2.**

Substrate	Catalyst	V_{max}	K_m	Slope	Intercept	$k_{cat}(h^{-1})$
3,5-Di-tButyl catechol [3,5-DTBC]	1	6.9999×10^{-8}	1.733×10^{-4}	2581.535	1.28699×10^{7}	25.19
	2	2.991×10^{-8}	1.01×10^{-3}	23346.928	3.73406×10^{7}	10.76

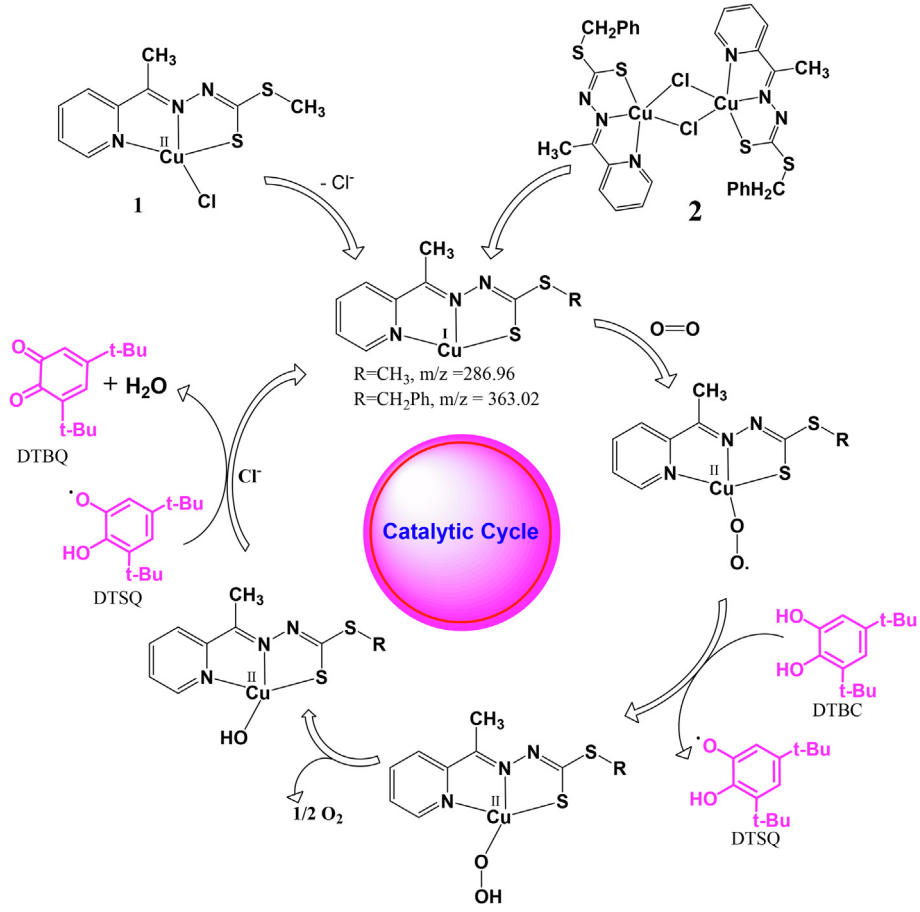

Scheme 2. Plausible mechanistic pathway for the oxidation of 3,5-DTBC by dioxygen in presence of catalyst complex **1** or complex **2**.

molecular oxygen. In the process of oxygen activation DTBC is transform to DTSQ (ditertiary butyl semiquinone) (Scheme 2). The peak corresponding to intermediate adduct [Cu(L)(DTBC)(O_2)] in the course of catalytic transformation are observed in the mass spectra of **1** and **2** in DTBC at *m*/*z* 539.12 (Fig. S4) and *m*/*z* + Na 639.40 (Fig. S5), respectively indicating the adduct formation between substrate, catalyst, and molecular oxygen. The catecholase activity of **1** is 2.5 times greater than the **2**. The low activity of **2** may be due to the high activation energy required to form $[CuL]^+$ intermediate breaking a dichloro dimeric structure. This fact is also supported by the weak dispersion interaction in the [Cu(L_2)Cl] layers due to the largeness of the phenyl moiety of L_2.

3.7. Molecular docking study

The binding mode of **1** and **2** with protein surface are shown in Figs. 12 and 13, respectively where the interactions of **1** and **2** with protein surface model are shown in Figs. 14 and 15 , respectively. The results indicate that complexes under investigation are well fitted in the active pocket of the protein molecule. Complex **1** exerts hydrophobic interaction with THR269, ARG267, VAL251, ALA249, CYS247, ASP286, VAL287, GLY288 and one hydrogen bonding interaction with LEU250 base pair of protein chain [57]. The free binding energy with protein is −5.52 kcal/mole and inhibition constant, Ki = 90.23 μM [at 298.15 K]. The calculated

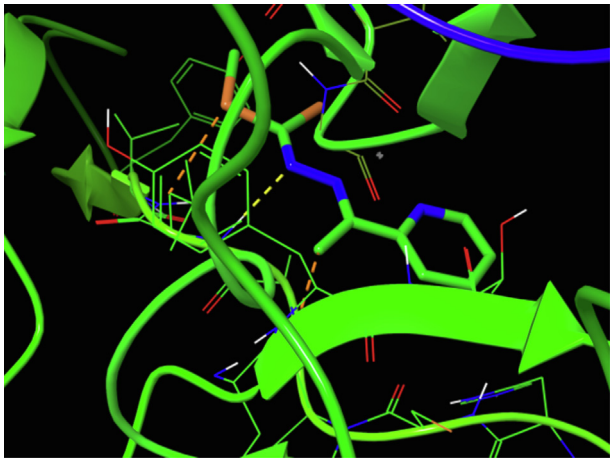

Fig. 12. Binding mode of **1** with Truncated ErbB2 Ectodomain. The protein was shown in surface. Complex was shown in sticks.

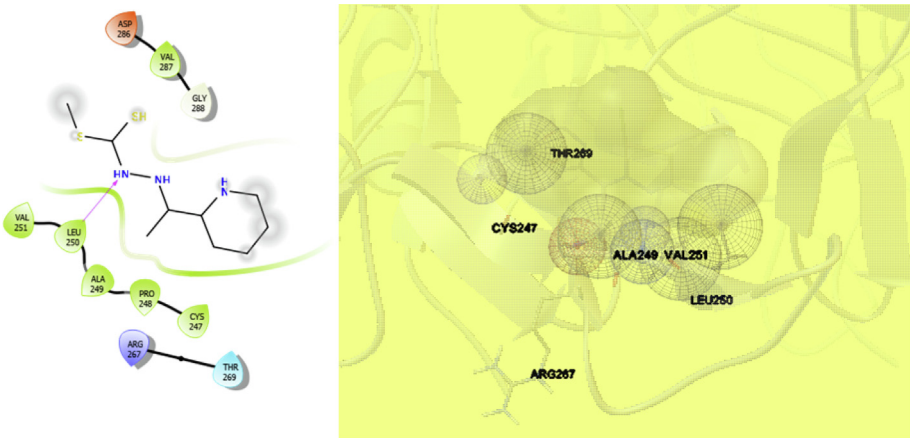

Fig. 13. Binding mode of **1** with Truncated ErbB2 Ectodomain. The protein was shown in surface. Complex was shown in solid sphere.

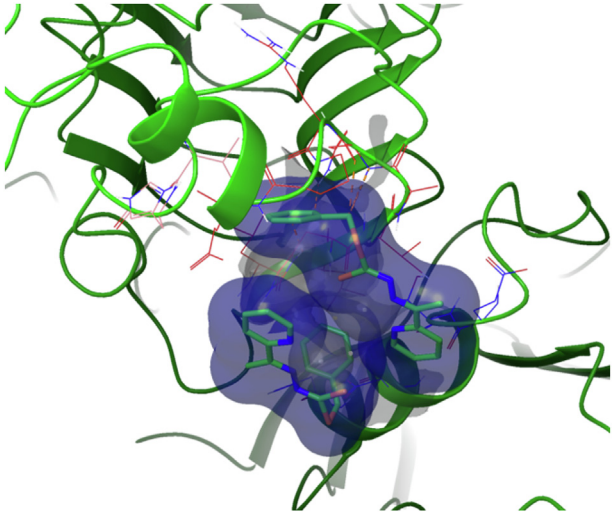

Fig. 14. Hydrophobic and hydrogen bond interaction of **1** with truncated ErbB2 Ectodomain protein.

intermolecular energy is −5.82 kcal/mole and summation of vdW, H-bond and dissolved energy is −5.77 kcal/mol. The electrostatic energy is calculated to −0.05 kcal/mol where the total internal energy is −0.04 kcal/mol and the torsional free energy is + 0.30 kcal/mole with unbound system's energy is −0.04 kcal/mole. Complex **2** also forms hydrophobic interaction with GLU480, PRO449, ARG478, ASN477, ALA476, THR475, HIS474 and GLU19 base pair of protein chain. The values of different computed weak interactions e.g., binding energy with protein (−8.04 Kcal/mol), inhibition constant (Ki = 1.28 μM at 298.15 K), intermolecular energy (−9.83 Kcal/mol), internal energy (−1.3 Kcal/mol), torsional energy (−1.79 Kcal/mole), and unbound extended energy (−1.3 Kcal/mole) are found in complex 2 with cluster RMS = 0.0 and reference RMS = 73.35. The docking evaluation of **1** and **2** with the target enzyme showed that weak interactions like hydrogen bonding and van der Waals forces are mainly responsible. The docking study could explain the potency of the complexes as an effective model of catecholase activity.

4. Conclusion

Copper(II) complexes with methyl-2-(1-(pyridin-2-yl)ethylidene)hydrazine-1-carbodithioate (HL_1) and benzyl-2-(1-(pyridin-2-yl)ethylidene)hydrazine-1-carbodithioate (HL_2) were synthesized and characterized by IR spectroscopy, X-ray crystallography, TGA. The stabilities of the monomeric and dimeric structures of these complexes were investigated computationally at the UB3LYP-D3 level. The mono nuclear structure of the [Cu(L_1)Cl] layers was found due to strong dispersion interaction between Cl and CH_3 moieties located at different layers. However, this interaction

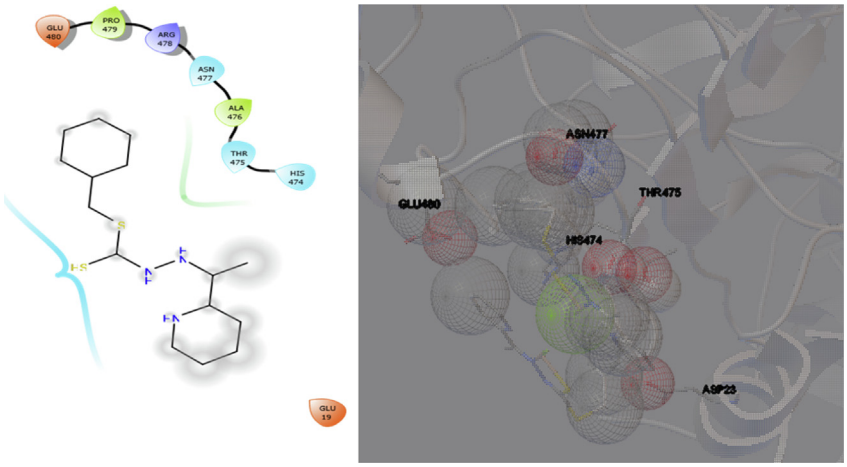

Fig. 15. Hydrophobic interactions of **2** with base pair of Truncated ErbB2 Ectodomain protein chain.

is hindered in the $[Cu(L_2)Cl]$ layers due to the largeness of the phenyl moiety of L_2 than the separation between the layers that prevents slide of the layers on top of each other. As a result, the strong electrostatic interaction between Cu and Cl atoms located at different layers results in chloro-bridged $[Cu(L_2)Cl]_2$ structure. Both monomeric $[Cu(L_1)Cl]$ and dimeric $[Cu(L_2)Cl]_2$ complexes act as a good catalyst to show catechol oxidase mimetic activity in methanol medium, through a fraction of $[CuL]^+$ species in methanol medium.

Acknowledgments

We gratefully acknowledge to Council for Scientific and Industrial Research (CSIR), Government of India for the project grant [No. 1 (2858)/16/EMR–II]. Panskura Banamali College (Autonomous) acknowledges the grants received from the Department of Science and Technology (SR/FST/College–295 dated 18/11/2015), Govt. of India through FIST program. We thank Syam Sengupta, IISER, Kolkata for EPR spectral analysis.

Conflict of interest

The authors declare that they have no conflict of interest.

Appendix A. Supplementary data

CCDC 1833374 and 1833376 for compound **1** and **2**, respectively. Crystallographic data can be obtained free of charge on application to CCDC, 12 Union Road, Cambridge CB2 1EZ, UK, fax: (+44) 1223 336033, e-mail: deposit@ccdc.cam.ac.uk. The computational structures are provided. Supplementary data to this article can be found online at https://doi.org/10.1016/j.poly.2019.114277.

References

[1] M.T.H. Tarafder, A.M. Ali, D.J. Wee, K. Azahari, S. Silong, K.A. Crouse, Transition Met. Chem. 25 (2000) 456.
[2] A.B. Beshir, S.K. Guchhait, J.A. Gascon, G. Fenteany, Bioorg. Med. Chem. Letters 18 (2008) 498.
[3] M.T.H. Tarafder, A. Kasbollah, K.A. Crouse, A.M. Ali, B.M. Yamin, H.K. Fun, Polyhedron 20 (2001) 2363.
[4] N.C. Kasuga, K. Sekino, M. Ishikawa, A. Honda, M. Yokoyama, S. Nakano, N. Shimada, C. Koumo, K. Nomiya, J. Inorg. Biochem. 96 (2003) 298.
[5] M.X. Li, L.Z. Zhang, C.L. Chen, J.Y. Niu, B.S. Ji, J. Inorg. Biochem. 106 (2012) 117.
[6] M. Shahid, M. Salim, M. Khalid, M.N. Tahir, M.U. Khan, A.A.C. Braga, J. Mol. Struct. 1161 (2018) 66.
[7] H. Zhou, D. Li, P. Wang, L. Cheng, Y. Gao, Y. Zhu, J. Wu, Y. Tian, Z. Tao, M. Jiang, H.K. Fun, J. Mol. Struct. 826 (2007) 205.
[8] P. Gómez-Saiz, R. Gil-García, M.A. Maestro, J.L. Pizarro, M.I. Arriortua, L. Lezama, T. Rojo, M. González-Álvarez, J. Borrás, J. García-Tojal, Inorg. Biochem. 102 (2008) 1910.
[9] D.X. West, A.E. Liberta, S.B. Padhye, R.C. Chikate, P.B. Sonawane, A.S. Kumbhar, R.G. Yerande, Coord. Chem. Rev. 123 (1993) 49.
[10] R. Vafazadeh, R. Esteghamat-Panaha, A.C. Willis, A.F. Hill, Polyhedron 48 (2012) 51.
[11] T.S. Lobana, R.J. Butcher, A. Castineiras, E. Bermejo, P.V. Bharatam, Inorg. Chem. 45 (2006) 1535.
[12] S. Walia, S. Kaur, J. Kaur, A.K. Sandhu, T.S. Lobana, G. Hundal, J.P. Jasinski, ZAAC 641 (2015) 1728.
[13] V. Philip, V. Suni, M.R.P. Kurup, M. Nethaji, Polyhedron 25 (2006) 1931.
[14] B.K. Koo, J. Korean Chem. Soc. 59 (2015) 103.
[15] P. Vijayan, P. Viswanathamurthi, K. Velmurugan, R. Nandhakumar, M.D. Balakumaran, P.T. Kalaichelvan, J.G. Malecki, RSC Adv. 5 (2015) 103321.
[16] M.A. Ali, A.H. Mirza, R.J. Butcher, M.T.H. Tarafder, T.B. Keat, A.M. Ali, J. Inorg. Biochem. 92 (2002) 141.
[17] A. Biswas, L.K. Das, M.G.B. Drew, G. Aromí, P. Gamez, A. Ghosh, Synth. Inorg. Chem. 51 (2012) 7993.
[18] L.K. Das, A. Biswas, J.S. Kinyon, N.S. Dalal, H. Zhou, A. Ghosh, Inorg. Chem. 52 (2013) 11744.
[19] K.S. Banu, T. Chattopadhyay, A. Banerjee, S. Bhattacharya, E. Suresh, M. Nethaji, E. Zangrando, D. Das, Inorg. Chem. 47 (2008) 7083.
[20] D. Kovala-Demertzi, P.N. Yadav, J. Wiecek, S. Skoulika, T. Varadinova, M.A. Demertzis, J. Inorg. Biochem. 100 (2006) 1558.
[21] K.M. Deck, T.A. Tseng, J.N. Burstyn, Inorg. Chem. 41 (2002) 669.
[22] L. Zhu, O. Santos, C.W. Koo, M. Rybstein, L. Pape, J.W. Canary, Inorg. Chem. 42 (2003) 7912.
[23] A. Biswas, L.K. Das, M.G.B. Drew, C. Diaz, A. Ghosh, Inorg. Chem. 51 (2012) 10111.
[24] S.K. Dey, A. Mukharjee, Coord. Chem. Rev. 310 (2016) 80.
[25] S. Dasgupta, I. Majumder, P. Chakraborty, E. Zangrando, A. Bauza, A. Frontera, D. Das, Eur. J. Inorg. Chem. (2017) 133.
[26] S. Dolai, K. Das, A. Bhunia, V. Bertolasi, S.C. Manna, Appl. Org. Chem. 32 (2018) 4506.
[27] A.D. Becke, J. Chem. Phys. 98 (1993) 5648.
[28] C. Lee, W. Yang, R.G. Parr, Phys. Rev. B 37 (1988) 785.
[29] A.D. Becke, Phys. Rev. A 38 (1988) 3098.
[30] P. Bera, C.-H. Kim, S.I. Seok, Polyhedron 27 (2008) 3433.
[31] Bruker, SMART (Version 5.625) Data Collection Program, Bruker AXS Inc., Madison, Wisconsin, USA (2001).
[32] Bruker, SAINT (Version 6.28a) and SADABS (Version 2.03) Data Reduction and Absorption Correction Program, Bruker AXS Inc., Madison, Wisconsin, USA (2001).
[33] G.M. Sheldrick, SHELXTL (Version 6.12) Structure Analysis Program, Bruker AXS Inc., Madison, Wisconsin, USA, 2001.
[34] F. Neese, The ORCA Program System, Wiley Interdiscip. Rev. Comput. Mol. Sci. 2 (2012) 73.
[35] F. Neese, Software Update: The ORCA Program System, Version 4.0, Wiley Interdiscip. Rev. Comput. Mol. Sci. 8 (2018) 1327.
[36] F. Weigend, Phys. Chem. Chem. Phys. 8 (2006) 1057.
[37] F. Weigend, R. Ahlrichs, Phys. Chem. Chem. Phys. 7 (2005) 3297.
[38] S. Grimme, S. Ehrlich, L. Goerigk, J. Comput. Chem. 32 (2011) 1456.
[39] F. Weigend, M. Häser, H. Patzelt, R. Ahlrichs, Chem. Phys. Lett. 294 (1998) 143.
[40] K. Eichkorn, O. Treutler, H. Öhm, M. Häser, R. Ahlrichs, Chem. Phys. Lett. 240 (1995) 283.
[41] V. Barone, M. Cossi, J. Phys. Chem. A 102 (1998) 1995.
[42] Z.L. You, Y.M. Cui, Y.P. Ma, C. Wang, X.S. Zhou, K. Li, Inorg. Chem. Comm. 14 (2011) 636.
[43] P.R. Reddy, A. Shilpa, N. Raju, P. Raghavaiah, Synthesis, structure, J. Inorg. Biochem. 105 (2011) 1603.
[44] S. Sarkar, A. Sim, S. Kim, H.I. Lee, J. Mol, Catal. A: Chem. 410 (2015) 149.
[45] A. Jana, P. Brandão, G. Mondal, P. Bera, A. Santra, A.D. Jana, R.B. Mokhamatam, S.K. Manna, P. Bera, Inorg. Chim. Acta 482 (2018) 621.
[46] L. Rigamonti, A. Forni, R. Pievo, J. Reedjijk, A. Pasini, Dalton Trans 40 (2011) 3381.
[47] M.S. Begum, E. Zangrando, M.C. Sheikh, R. Miyatake, M.B.H. Howlader, M.N. Rahman, A. Ghosh, Transition Met. Chem. 42 (2017) 553.
[48] J.-L. Chen, Z.-H. Guo, H.-G. Yu, L.-H. He, S.-J. Liu, H.-R. Wena, J.-Y. Wang, Dalton Trans. 45 (2016) 696.
[49] M.F. Haddow, H. Kara, G.R. Owen, Inorg. Chim. Acta 362 (2009) 3502.
[50] Y. Acar, H. Kara, E. Gungor, M.B. Coban, Mol. Cryst. Liq. Cryst. 664 (2018) 165.
[51] M. Atanasov, P. Comba, B. Martin, V. Müller, G. Rajaraman, H. Rohwer, S. Wunderlich, J. Comput. Chem. 27 (2006) 1263.
[52] S. Kundu, A. Mondal, T. Weyhermüller, S. Sproules, P. Ghosh, Inorg. Chim. Acta 451 (2016) 23.
[53] S. Grimme, R. Huenerbein, S. Ehrlich, Chem. Phys. Chem. 12 (2011) 1258–1261.
[54] P. Chakraborty, I. Majumder, H. Kara, S.K. Chattopadhyay, E. Zangrando, D. Das, Inorg. Chim. Acta 436 (2015) 139.
[55] I. Majumder, P. Chakraborty, J. Adhikary, H. Kara, E. Zangrando, A. Bauza, A. Frontera, D. Das, Chemistry Select 3 (2016) 615.
[56] A. Jana, P. Brandão, H. Jana, A.D. Jana, G. Mondal, P. Bera, A. Santra, A.K. Mahapatra, P. Bera, J. Coord, Chem. 72 (2019) 2636.
[57] M.M. Abd-Elzaher, A.A. Labib, H.A. Mousa, S.A. Moustafa, M.M. Ali, A.A. El-Rashedy, Beni-suef Univ. J. Basic Appl. Sci. 5 (2016) 85.